Journal of Photochemistry, 13 (1980) 295 - 307

PICOSECOND TIME RESOLUTION BY A CONTINUOUS WAVE LASER AMPLITUDE MODULATION TECHNIQUE II: EXPERIMENTAL BASIS

HEINRICH GUGGER and GION CALZAFERRI

Institute for Inorganic and Physical Chemistry, University of Bern, Freiestrasse 3, CH-3012 Bern (Switzerland)

(Received January 24, 1980)

Summary

Based on a theoretical investigation, which can be used for several similar procedures, we present the experimental and instrumental features of our specific method for determining luminescence lifetimes in the picosecond domain. The intensity-modulated light of a continuous wave laser is used to induce a phase shift between excitation and emission of the sample under study. As in phase fluorimetry, this shift is measured and is related to the luminescence lifetime. The absolute accuracy of the lifetimes ranges from 30 to 50 ps for our set-up. Relative determinations can be performed to within ±15 ps. It should be stressed that this technique works at low laser power levels.

1. Introduction

1.1. Objective

The concept of measuring short lifetimes using intensity-modulated light has occupied many minds. Phase fluorimetry performed with conventional lamps has already led to astonishingly accurate results. Birks and Munro [1] have summarized its development up to 1967 and recent studies [2] emphasize the steady interest in this technique. With the advent of laser technology, phase fluorimetry has received new impulses through different approaches [3]. They all have the same theoretical basis [4].

A luminescent sample excited by sinusoidally intensity-modulated light emits intensity-modulated luminescence. The modulation angular frequency ($\omega = 2\pi\nu$) is conserved, but the modulation depth shrinks and the emission is delayed with respect to the excitation. This delay can be measured as a phase shift Φ_τ. For single exponential decays Φ_τ is related to the luminescence decay time τ by

$$\omega\tau = \tan \Phi_\tau$$

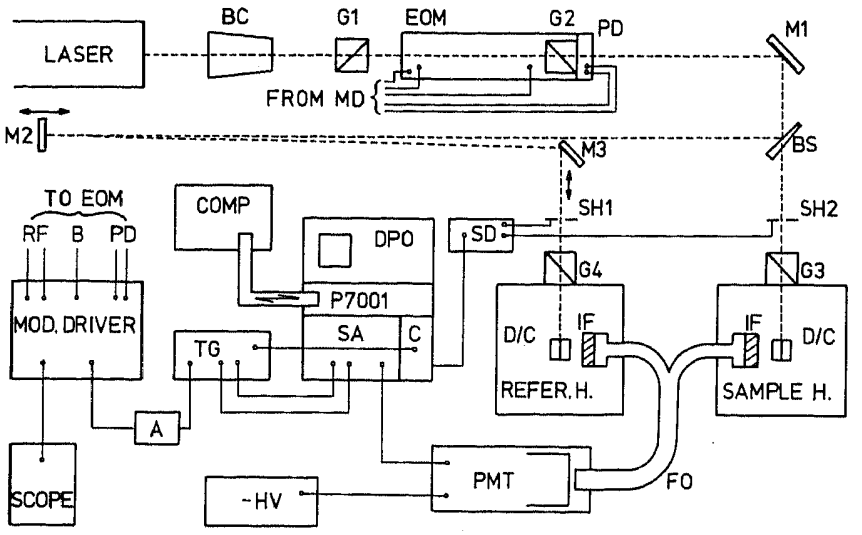

Fig. 1. The experimental layout: - - -, laser beam; o——o, electrical connections. Optics: BC, beam collimator; G1 - G4, Glan prism polarizers; M1 - M3, mirrors; BS, beam splitter; IF, interference filter; FO, fibre optics. Electronics: DPO, digital processing oscilloscope; P7001, processor of the DPO; COMP, minicomputer; SA, spectrum analyser plug in; C, counter plug in; TG, tracking generator; A, amplifier; SD, shutter driver; PMT, photomultiplier; HV, high voltage supply. Modulator: EOM, electro-optical modulator; PD, photodiode assembly; MD, modulator driver; RF, output and termination of r.f. driving voltage; B, bias voltage. Housings: REFER. H., reference chamber; SAMPLE H., sample chamber; D/C, diffuser or cuvette.

Thus the experiment has to yield exact values for Φ_τ within a certain frequency interval. This enables investigations of multistep processes to be carried out.

1.2. Experimental layout

The laser beam (Fig. 1) is intensity modulated by the electro-optical modulator (EOM). It is then split (at BS) into two beams; the transmitted part enters the sample chamber, whereas the reflected part serves as a phase reference and is directed along an optical delay line into the reference housing. In both housings the light either excites a sample or is simply scattered. Narrow-band dielectric filters (IF) select whether emitted or scattered light should fall onto the entrance of the receiving arm of the fibre optics (FO). The optical fibres of both arms are joined, mixed and guided to the photomultiplier. The anode current thus generated is Fourier transformed in a spectrum analyser, digitized and analysed using a minicomputer.

2. Instrumentation

2.1. Along the light path

The light source used is a krypton ion gas laser (Spectra Physics, Model 171) operating with single-line option. The beam is collimated to ensure a clean throughput across the modulator crystals. The polarization is then up-

graded by means of a Glan prism (G1) since the modulation depth depends markedly on the degree of polarization. The modulation is performed using a Coherent Associates 3050 electro-optical modulation system. It is necessary to isolate the modulator body electrically from the mounting elements in order to reduce undesired radiation scatter.

An uncoated quartz wedge splits the modulated beam into a transmitted beam (approximately 90%) which enters the sample chamber and into a low intensity portion (approximately 5%) which is deflected to the optical delay line. To avoid disturbing the original modulation phase by multiple paths, we use a wedge which distinctly separates the front-side and back-side reflexes at the air–quartz junction. The delay line length is varied by changing the position of the mirror M2. The geometry is preserved by an appropriate adjustment of the mirror M3. Each of the polarized beams prepared in this manner passes the Glan prism (G3 or G4) acting as a variable power attenuator at the entrance of the housing. The housings are identical and both are fitted with two precisely positionable and interchangeable mounts to take up the incoming laser light. The first mount simply holds a sample cuvette. The second mount contains a magnesium oxide diffuser which is inserted nearly parallel to the beam and acts as a reflector. We thus achieve equivalent geometric conditions for the luminescence emission in a sample cuvette and for the beam reflected by the diffuser. These geometric considerations are very important since the photons still travel approximately 3 mm in 10 ps. Unwanted scattered light of the excitation wavelength is eliminated by interchangeable narrow-band dielectric interference filters (Balzers) which are placed in close contact to the front end of the optical fibres. To provide optimum light collection both arms are furnished with a rectangular entrance profile (2 mm × 7 mm) parallel to the laser beam. We abandoned the use of focusing optics since they can yield false time-of-flight statistics in the picosecond domain. The two arms are then united to a single cable in which the individual fibres are statistically mixed before they reach the circular outlet for the light.

This concept of guiding the light to a spot ($\phi \approx 8$ mm) at the centre of the photomultiplier eliminates cathode non-uniformity problems arising from slight beam deviations during and between two phase determinations. Moreover, the light path from the housings to the photomultiplier is held fixed and hence requires no readjustments. Compared with full-size illumination of the cathode, the centre spot illumination reduces the electron transit time spread. Large spreads decrease the contrast ratio of the modulated signal. Highest accuracy according to earlier work [5] is given at $\Phi_i \approx \pi$, where the phase difference between the reference beam and the sample beam is nearly π. This means that the photomultiplier detects only a very weak a.c. component on a high d.c. level. The mean average current, at which most photomultipliers can be operated linearly without damage or reaching the saturation point, ranges from about 1 to about 100 μA. If the modulation depth is poor an extra d.c. component is added, clipping the relative sensitivity on all a.c. signals. We use a five-stage RCA 31024 head-on tube

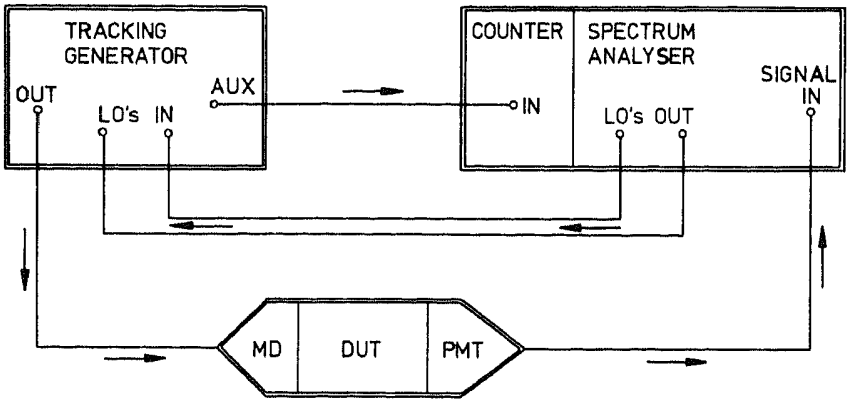

Fig. 2. The synchronism concept: ——►, information flux; DUT, device under test (includes the electronics and light phenomena from MD to PMT); MD, modulator driver; PMT, photomultiplier tube.

designed for transient experiments. The total anode current released can be regulated at the light-attenuating Glan prisms (G3 and G4) and is maintained at 2 - 3 μA. For matched anode circuits of 50 Ω impedance this corresponds to microvolt signals.

2.2. Acquisition

Data acquisition is based on the Tektronix WP 2222 waveform processing system in conjunction with a digital processing oscilloscope (DPO). The DPO is equipped with a built-in processor (P7001) including a memory block to store four independent traces complete with scaling and read-out information. The horizontal resolution is 512 points per trace at a vertical dynamic range of 1024 points. An interesting feature of this system is the software-controlled signal averaging in the P7001; this provides a continuous and fast acquisition, since the more time-consuming data transfer from the processor to the minicomputer (PDP 11-05) takes place only at the end of the acquisition procedure.

The electrical signal analysis is performed by two plug-in units to the DPO: a 7L13 spectrum analyser and a 7D14 digital frequency counter.

2.3. Frequency synchronism

The 7L13 spectrum analyser offers a 30 Hz resolution for frequency settings up to 1.8 GHz. Taking advantage of this high resolution enhances the signal-to-noise ratio, but it also limits the frequency band which can be swept at reasonably fast sweep speeds. These narrow bands imply excellent frequency stability of all circuits. An experimental difficulty arises here. The point on the frequency axis of the spectrum analyser which coincides with the modulation frequency must be determined, since the signal magnitude yields significant information only at this point. Because the spectrum analyser enables only relative frequency determinations to be made with high precision, the foregoing requirements can only be approximated. Therefore we replaced our sine-wave generator by a tracking generator (Tektronix

TR501) which synchronizes excitation and detection (Fig. 2). The tracking generator continuously reads the actual detection frequency of the spectrum analyser from the local oscillators (LOs). Because of this it simultaneously synthesizes a sine-wave; the generator permanently tracks the frequency sweeps of the analyser.

In our experiment the system can be operated at a single frequency. Accordingly the DPO screen displays the time domain behaviour of the signal magnitude. In this mode the spectrum analyser acts as a frequency-selective level meter for signal strengths down to −70 to −90 dBm against noise levels which in this configuration range from −110 to −130 dBm, providing a high signal-to-noise ratio. Fluctuations and drifts are easily recognized along the sweep. Moreover, the signal-to-noise ratio is improved since all 512 points of one sweep can be interpreted instead of only one point.

2.4. Procedure control

Once the set-up has been optically and electronically adjusted, experimental control is passed to the user software which asks for complementary instructions concerning the signal averaging. The software also controls the beam selection during the acquisition cycles, operating the electromagnetic shutters by sending the "Single Sweep Reset" command to the DPO. The dummy command is converted to the driving voltages required by the shutters. This automation keeps the measurement intervals constant and reduces dead time during data transfer to a minimum.

3. Experimental

A luminescence decay time τ is determined as the phase difference $\Phi_\tau = \Phi_1 - \Phi_0$. The measurement procedure for the phase Φ_i ($i = 0, 1$) is identical; however, for Φ_1 the scatterer is replaced by the sample.

3.1. Phase measurement

In the theoretical investigation [5] we have described the background of the four-step acquisition cycle which is required for the determination of Φ_i involving the measurement of (1) the reference level, (2) the sample level, (3) the sum signal level and (4) the noise level. The error discussion [5] has revealed that the uncertainty in the spectrum analyser reading causes the greater portion of the total phase error. Therefore a calibration procedure has been established to decrease this uncertainty: prior to the phase measurement the output of the tracking generator is connected to an external variable attenuator (Tektronix 2701) which is linked to the input of the spectrum analyser, thus simulating conditions which are equivalent to the real acquisition conditions. The attenuation is set in line with the reference level of the spectrum analyser prepared for the determination of Φ_i. The attenuation is then increased in 1 decibel steps across the whole screen (14 decibels). Every step is acquired. Instead of readjusting the linear and loga-

rithmic potentiometers of the internal amplifiers, correction of the signal level reading is performed numerically by a software subroutine. Once the screen calibration is established, we determine the noise level at the measurement frequency while both shutters are closed and no light falls onto the photomultiplier. Then the program starts the acquisition loop of the modulated signals (1) - (3). Every level is averaged in one of the memory locations of the P7001 during about 5 s. This corresponds to approximately 30 sweeps at rates of 100 - 200 ms sweep^{-1}. The intermissions between level changes are used to acquire the actual frequency read-out of the counter. When the processor memory contains the three average traces (1) - (3), all data are transferred to the minicomputer. The waveforms are reduced to single values and their root mean square errors are calculated. The shutters are then reset and the next cycle starts. Experience has led us to acquire 5 - 10 such cycles to obtain good results. Lengthening the measurement intervals or increasing the number of cycles often leads to deviations caused by instabilities of laser power, tracking adjustment or modulator bias.

3.2. Acquisition example

To determine the coherency of the experimental procedure and the applicability of the error estimation, we present a typical phase measurement in Table 1. Reference should be made to the theoretical investigation [5] for the exact physical meaning of the parameters listed.

The determination includes five cycles of 32 sweeps on each level. Every cycle represents a complete and independent measurement. At the given modulation angular frequency ($\omega = 2\pi\nu$) of 197.284 MHz the observed phase shift Φ_i is 3.3745 rad. Taking into account the velocity of light we convert this phase shift to a path length L which equals the delay distance between the sample path and the reference path. The mean value of the measured phase shift corresponds to a distance of 513.14 cm. When cycles 1 - 5 in this block (L) are considered, a small systematic lengthening can be seen. This usually occurs because of small drifts in the tracking adjustment or the laser parameters and because of a temperature change in the working area. The reproducibility is nevertheless very good: ±1.3 mm for the path length and ±0.89 mrad for the phase shift.

The error estimation yields 4.22 mrad for $d\Phi$ and 6.4 mm for dL. This phase error is composed of the following two parts: (1) $d\Phi_{\alpha,\beta}$ which arises from the uncertainties $d\alpha$ and $d\beta$ in the parameters α and β; (2) $d\Phi_\gamma$ which arises from the signal-to-noise ratio measured as γ. The mean signal-to-noise ratio in our example is 35.5 decibels and causes an error of 2.44 mrad.

Information about the errors on the time scale corresponding to the phase errors are given by $d\tau_{\alpha,\beta}$, $d\tau_\gamma$, $d\tau_\Phi$, $d\tau_\omega$ and $d\tau$. The time error $d\tau_\omega$, which is dependent on the frequency accuracy, is negligible in our set-up.

The phase error $d\Phi$ and consequently the time error $d\tau_\Phi$ of cycle 1 appear to be unusually high. The reason for this can be seen from examination of the block $d\beta$. Since the value for $d\alpha$ is normal, it follows from the definition of α and β that the physical stability of the acquired sum signal is

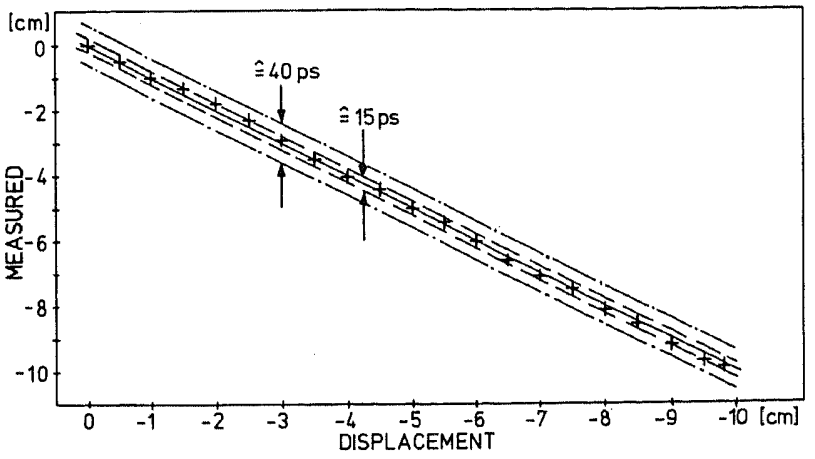

Fig. 3. A resolution test for $\Phi_\tau \approx 0.6$ rad at $\nu = 28.8$ MHz: +, measured values; ——, theoretical line tracing the exact course of a continuous displacement of the mirror M2 (Fig. 1); — — —, delimits the band in which all the experimental points lie (100% relative error of experimental points); — · — ·, absolute error which follows from the error estimation.

poor. This specific example demonstrates how a complete data set helps to judge the single measurements at any time.

3.3. *Results*

The manner in which we apply the optical delay line yields a precise evaluation of the time resolution in every experiment.

The position of the displaceable mirror M2 (Fig. 1) sets the phase Φ_0 at the given modulation angular frequency ω. To minimize errors this mirror has to be adjusted in a manner such that $\Phi_0 \approx \pi + \Phi_\tau/2$ is satisfied. For short luminescence lifetimes the phase shift Φ_τ fulfills the condition $\Phi_\tau \ll (\Phi_0, \Phi_1)$. The resolution test should be made at a corresponding small phase shift $\Delta\Phi$ (less than Φ_τ). These $\Delta\Phi$s can be produced by exactly known displacements of the mirror M2. After each move a complete determination of Φ_0 must be performed. The measured phase Φ_0 is converted to the corresponding path length of the optical delay. The length differences should equal the effected displacement of the mirror M2. Figure 3 shows such a resolution test. The modulation frequency ν is 28.8 MHz and Φ_τ is approximately 0.6 rad. This corresponds to the resolution possibilities for samples with decay times of about 4 ns. The time resolution increases to a certain limit [5] for samples with smaller decay times.

Each experimental point of Fig. 3 is documented in Table 2. It should be noted that the reproducibility $\pm L$ (see also Table 1) of every point is much better (less than 5 ps) than the absolute accuracy dL or, if the time domain is considered, $d\tau$ (approximately ±20 ps). The relative precision among several measured phases lies in between and is better than ±10 ps (see also Fig. 3). It is noticeable that even the reasonably good signal-to-noise ratio of 40 decibels contributes one-half to the total phase error ($d\Phi_\gamma/d\Phi \approx \frac{1}{2}$). Since we assume a gaussian distribution, the error $d\Phi_\tau$ of a complete lifetime measurement is given by

TABLE 1

A typical five-cycle phase determination

Cycle number[a]	Φ_i (rad)	γ (10 decibels)	L (cm)	α (20 decibels)	β (10 decibels)
1	3.37316	−3.55074	512.939	−0.0112167	−1.27841
2	3.375	−3.55317	513.219	-8.50563×10^{-3}	−1.27118
3	3.37375	−3.55299	513.029	-8.78220×10^{-3}	−1.27587
4	3.37481	−3.55378	513.191	-7.57370×10^{-3}	−1.27157
5	3.37562	−3.55612	513.313	-6.66351×10^{-3}	−1.26824
M	3.37447	−3.55336	513.138	-8.54835×10^{-3}	−1.27306
±	8.89334×10^{-4}	1.72151×10^{-3}	0.135466	1.52835×10^{-3}	3.61707×10^{-3}
Cycle number[a]	$d\Phi_{\alpha,\beta}$ (rad)[b]	$d\Phi_\gamma$ (rad)[b]	dL (cm)[b]	$d\alpha$ (20 decibels)	$d\beta$ (10 decibels)
1	6.43874×10^{-3}	2.44237×10^{-3}	1.04718	5.48864×10^{-3}	0.023745
2	2.02428×10^{-3}	2.44237×10^{-3}	0.48238	4.89153×10^{-3}	7.31651×10^{-3}
3	3.27418×10^{-3}	2.44237×10^{-3}	0.621151	5.52424×10^{-3}	0.0120224
4	2.11563×10^{-3}	2.44237×10^{-3}	0.491361	4.90373×10^{-3}	7.59796×10^{-3}
5	2.80777×10^{-3}	2.44237×10^{-3}	0.565893	4.95972×10^{-3}	0.0100962
M	3.33212×10^{-3}	2.44237×10^{-3}	0.641593	5.15357×10^{-3}	0.0121556
±	1.61986×10^{-3}	0	0.209077	2.89250×10^{-4}	6.04585×10^{-3}
Cycle number[a]	$d\tau_{\alpha,\beta}$ (s)[b]	$d\tau_\gamma$ (s)[b]	$d\tau_\Phi$ (s)[b]	$d\tau_\omega$ (s)[b]	$d\tau$ (s)[b]
1	3.44514×10^{-11}	1.30683×10^{-11}	3.68467×10^{-11}	1.46607×10^{-15}	3.68467×10^{-11}
2	1.08407×10^{-11}	1.30797×10^{-11}	1.69882×10^{-11}	3.05749×10^{-15}	1.69882×10^{-11}
3	1.75239×10^{-11}	1.30719×10^{-11}	2.18623×10^{-11}	2.07456×10^{-15}	2.18623×10^{-11}
4	1.13289×10^{-11}	1.30785×10^{-11}	1.73029×10^{-11}	2.54351×10^{-15}	1.73029×10^{-11}
5	1.50410×10^{-11}	1.30835×10^{-11}	1.99351×10^{-11}	3.74697×10^{-15}	1.99351×10^{-11}
M	1.78372×10^{-11}	1.30764×10^{-11}	2.25871×10^{-11}	2.57772×10^{-15}	2.25871×10^{-11}
±	8.66326×10^{-12}	5.51783×10^{-15}	7.35073×10^{-12}	7.85804×10^{-16}	7.35073×10^{-12}

Cycle number[a]	*Argument E*	ω (Hz)	$d\omega$ (Hz)	$d\Phi$ (rad)[b]
1	−0.973308	1.97284×10^{8}	15.0299	6.88640×10^{-3}
2	−0.972884	1.97284×10^{8}	31.2872	3.17220×10^{-3}
3	−0.973172	1.97284×10^{8}	21.2555	4.08478×10^{-3}
4	−0.972927	1.97284×10^{8}	26.0325	3.23126×10^{-3}
5	−0.97274	1.97284×10^{8}	38.3188	3.72139×10^{-3}
M	−0.973006	1.97284×10^{8}	26.3848	4.21921×10^{-3}
±	2.05147×10^{-4}	120.797	8.02275	1.37492×10^{-3}

[a]The data specific to each measurement cycle are indexed 1 - 5; M represents the arithmetic mean of the five measurements; ± signifies the root mean square error of the five measurements.
[b]These data result from the error calculations and do not represent measured quantities.

TABLE 2

Data complementary to the displacement measurements[a]

$-D$ (mm)	$-L$ (mm)	$\pm L$ (mm)	$\pm dL$ (mm)	$\pm d\tau$ (ps)	Φ (rad)	$\pm d\Phi$ (mrad)	$\pm d\Phi_\gamma$ (mrad)	S/N (decibels)
28.8 MHz data[b]								
0.0	0.0	1.81	6.02	22.4	3.46611	3.64	1.83	40.7
5.0	5.0	0.90	5.54	20.5	3.46306	3.34	1.81	40.7
10.0	9.8	0.85	5.80	21.4	3.46020	3.50	2.06	39.5
15.0	12.9	1.32	5.63	20.8	3.45831	3.40	1.83	40.5
20.0	18.0	1.48	5.53	20.4	3.45520	3.34	1.71	41.2
25.0	23.2	2.01	4.73	17.4	3.45209	2.86	1.43	42.6
30.0	29.3	0.99	4.94	18.1	3.44839	2.98	1.39	42.7
35.0	35.2	1.23	4.78	17.5	3.44481	2.89	1.43	42.3
40.0	40.4	2.21	5.97	21.8	3.44168	3.60	2.49	37.5
45.0	44.3	1.45	4.56	16.6	3.43933	2.75	1.44	42.1
50.0	50.2	1.36	5.48	19.9	3.43577	3.31	2.00	39.3
55.0	54.4	2.34	5.31	19.3	3.43325	3.21	1.64	40.8
60.0	60.2	0.88	5.08	18.4	3.42976	3.07	1.65	40.8
65.0	66.2	1.82	5.12	18.5	3.42622	3.09	1.73	40.2
70.0	71.2	0.94	4.32	15.6	3.42310	2.61	1.47	41.5
75.0	75.0	2.39	5.17	18.6	3.42078	3.12	1.76	39.8
80.0	81.4	1.02	4.87	17.5	3.41693	2.94	1.82	39.4
85.0	85.7	1.44	5.00	18.0	3.41432	3.02	1.52	40.9
90.0	91.9	0.61	4.98	17.9	3.41058	3.01	1.55	40.6
95.0	97.0	1.18	5.68	20.3	3.40753	3.43	1.65	40.0
95.8	98.8	1.18	6.06	21.7	3.40646	3.66	1.70	37.0
36.3 MHz data[c]								
0	0	3.40	9.37	61.3	3.91725	7.13	1.52	47.7
1580	1602	0.5	7.00	28.6	2.69777	5.32	1.62	44.1

[a] D, displacement performed; L, displacement measured; dL, theoretical error of L; $\pm L$, root mean square error of L (10 cycles); Φ, phase measured; $d\Phi$, total phase error; $d\Phi_\gamma$, signal-to-noise share of phase error; S/N, signal-to-noise ratio.
[b] 28.8 MHz data completing Fig. 3.
[c] An example of the large delay length change determination at 36.3 MHz.

$$d\Phi_\tau = \left(\sum_i d\Phi_i^2\right)^{1/2}$$

With regard to the future treatment of multiexponential decay analysis [6], resolution has to be preserved within a certain band of modulation frequency at a given position of the mirror M2. To check to what extent our experiment is consistent with the error estimation, we performed the measurement series discussed in Fig. 3 at six different frequencies. Instead of 26 closely spaced points (Δ = 5 mm) as in Fig. 3, three mediumly spaced mirror positions were chosen (Δ = 40 mm). The mirrors are adjusted by a micrometer translation stage in order to provide exact reproducibility. The measured values (x) *versus* the displacement performed are shown in Fig. 4(a).

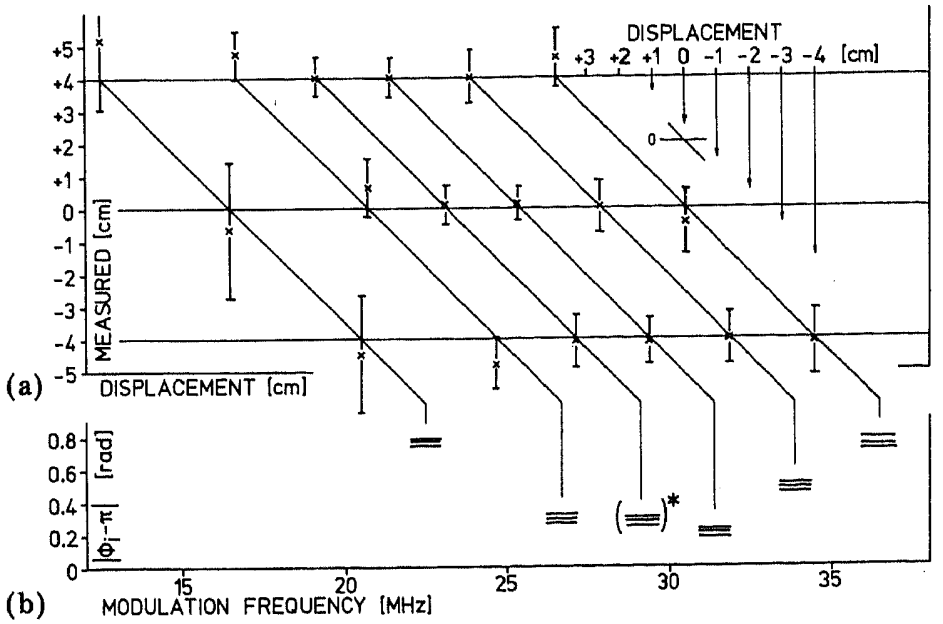

Fig. 4. Optical delay length variations at different modulation frequencies: (a) measured *vs.* effected displacements at +4, 0 and −4 cm; (b) the difference $|\Phi_i - \pi|$ as a function of the modulation frequency at a fixed position of the mirror M2. (*, denotes an exception explained in the text.)

The skeleton of the graph is built up from the six theoretical 45° lines and the three horizontal lines at +4, 0 and −4 cm. The intersection of two such lines locates the exact theoretical value of the specific measurement. As an example the 36 MHz determination is explained in detail at the upper right-hand corner of the plot. The "vertical parts of the 45° lines" indicate the modulation frequency at which the corresponding measurements have been carried out. Thus the spacing between measurement series of different frequency in Fig. 4(a) reflects the frequency differences between these series. This helps to bring the size of the error intervals in relation to the frequency and to the phase range. Towards 29 - 31 MHz it can be seen that the measured values lie closer to the theoretical values. This fact together with a detailed analysis similar to that shown in Table 1 confirm the reliability of our error estimation. The three horizontal bars at every frequency in Fig. 4(b) represent the phases of the three measured values with respect to π.

The difference $|\Phi_i - \pi|$ is a relevant criterion for the expected error. Measurements where $|\Phi_i - \pi|$ is smaller than 0.5 rad generally lead to precise results. Two comments should be made here. Although at 27 MHz the deviation of the measured values from the theoretical line are quite considerable, the calculated error intervals do at least touch the theoretical line. The determinations at 29 MHz have been made earlier at another delay line length. That is the reason why the three bars do not fit the general tendency in Fig. 4(b).

Up to now only short or medium displacements have been investigated. Longer displacements are more difficult for geometric stability reasons. Table 2 shows the result of such long-displacement measurement. For the

determination of a luminescent sample, we never have to displace optical elements during the determination; hence those measurements are more accurate.

4. Discussion

In this more technical paper the experimental aspects of our picosecond method are described in detail; the method relies on an easily understood physical concept. In this respect we want to draw the attention of the reader particularly to the extreme simplicity of the light path. The manner in which we use the optical delay line provides a valuable control of the time resolution, whereas the straightforward concept with its few essential measurement parameters enables a reasonable error estimation. On this basis we achieve a high and reliable time accuracy. The coupling between expected and observed deviations is very satisfying. We distinguish three types of measurement precision: absolute accuracy (30 - 50 ps), reproducibility (approximately 5 ps) and relative precision against a standard (10 - 15 ps). These values apply to short decay times ($\tau \leqslant 4$ ns) and do not include the error arising from the change of photomultiplier electron transit time due to different incident spectral light distributions. This error, however, does not appear in relative determinations, such as quenching rates, concentration series or solvent effects. To maintain the aforementioned accuracies even for decay times larger than 4 ns, the extraordinary beam at the exit of the modulator can be used as a phase reference. This reduces the delay line length required to the amount for $\Phi_\tau/2$.

We believe that the limit for the absolute time resolution is not entirely reached. The present state of the experiment, however, already allows the treatment of multistep processes. A numerical algorithm including the necessary error estimation has been established [6] for the set-up presented.

Acknowledgments

We would like to thank Professor Dr. E. Schumacher for his steady and constructive support of this work. Dr. S. Leutwyler advised us in many experimental aspects. Martin Gygax realized the constructions needed. This work was financed by the Swiss National Science Foundation (Grant No. 2.157.78).

References

1 J. B. Birks and I. H. Munro, *Prog. React. Kinet.*, *4* (1967) 239–303, and references cited therein.

2 K. Schurer, P. G. F. Ploegaert and P. C. M. Wennekes, *J. Phys. E*, *9* (1976) 821, and references cited therein.

3 H. P. Haar, U. K. A. Klein, F. W. Hafner and M. Hauser, *Chem. Phys. Lett.*, *49* (1977) 563.
E. R. Menzel and Z. D. Popovic, *Rev. Sci. Instrum.*, *49* (1978) 39.
E. W. Schlag, H. L. Selzle, S. Schneider and J. G. Larsen, *Rev. Sci. Instrum.*, *45* (1974) 364.
4 M. Eigen and L. de Maeyer, in *Techniques of Chemistry*, Vol. VI, Wiley, New York, 1974.
5 H. Gugger and G. Calzaferri, *J. Photochem.*, *13* (1980) 21.
6 H. Gugger and G. Calzaferri, Picosecond time resolution by a continuous wave laser amplitude modulation technique: III, to be published.